DOI: https://doi.org/10.33103/uot.ijccce.23.2.4

Sensorless Speed Control for PMSM Based on Multi-Level SVPWM Inverter and MRAS

Ruaa S. Hassan[1] , Farazdaq R. Yaseen[2]
[1,2]Control and Systems Engineering Department, University of Technology, Baghdad, Iraq
[1]cse.19.14@grad.uotechnology.edu.iq, [2]Farazdaq.R.Yaseen@uotechnology.edu.iq

Abstract— *Permanent Magnet Synchronous Motors (PMSM) are extensively used in the industry owing to their excellent efficiency, low weight/power ratio, and smooth torque with no or minimal ripple. Field Oriented Control (FOC) is a modern and effective approach for closed-loop controlling the speed of PMSM. In this paper, three-level Space Vector Pulse Width Modulation (SVPWM) is proposed for minimizing harmonics in the output voltage inverter. sensorless approaches are performed by using Model Reference Adaptive System (MRAS) which eliminates mechanical uncertainties. Because mechanical sensors increase the cost, size, weight, and wiring complexity, employing PMSM with them is extremely difficult Tuning of Proportional Integral (PI) controller gains is performed by using the Whale Optimization Algorithm (WOA). The results show that the proposed controller enhances the system's performance. In the application of felid-oriented control to a PMSM, with simulation data to back it up the entire system is simulated using the MATLAB/Simulink tool.*

Index Terms— *PMSM, SVPWM, FOC, MRAS, WOA.*

I. INTRODUCTION

Multi-level converters provide voltage levels greater than two. Additionally, the Multi-Level Inverter's (MLI) overall architecture may balance the amount of effort in itself, regardless of the drive control and load factors [1]. Inverters with many levels were first released in 1981 [2]. Multi-level inverters are becoming more common in applications requiring medium and high power. In comparison to conventional two-level inverters, multi-level inverters offer the following benefits: lower dv/dt, improved output performance, and reduced switching frequency [3]. The three primary MLI topologies are cascaded H-bridge inverters, diode-clamped inverters, and flying capacitors [4]. The most often used modulation methods for multi-level inverters are Space Vector Modulation (SVM) and Carrier-based Sinusoidal Pulse-Width Modulation (SPWM). Systems based on the SPWM algorithm are much easier to set up and provide output Total Harmonic Distortion results that are almost identical (THD). SVM methods, on the other hand, are more crucial than conventional SPWM methods because they produce higher amplitude modulation indices while reducing commutation losses and the harmonic content of the output voltage. Using digital processors, SVM techniques are also straightforward to implement [2].

PMSM, one type of electrical motor, has recently gained popularity in several important applications. This is because of their advantages and attributes, which are particularly useful for applications with a medium- or lower grade. Among these applications are those for electric vehicles, drive motion control, and industrial settings. The absence of a coil in the rotor for direct current excitation is replaced with a permanent magnet. The PMSM is more efficient due to its minimal rotor copper power loss, greatest torque-to-weight ratio, lightweight in comparison to other synchronous motor types, and small size [5].

The FOC and Direct Torque Control (DTC) are just two examples of the several operation schemes that have been developed and have come to be considered "standard" for the control of the PMSM [6].

Received 01/June/2022; Accepted 18/July/2022
© 2017 University of Technology, Iraq ISSN (Print) 1811-9212 ISSN (Online) 2617-3352

DOI: https://doi.org/10.33103/uot.ijccce.23.2.4

Sensors put on the motor are frequently used to assess rotor speed, which raises the system's cost and volume while lowering reliability. Sensorless control has been presented as a way to tackle this issue. Sensorless control systems use stator currents and stator voltages to estimate rotor speed and rotor angle. The observation is frequently utilized when the motor is running at high speeds and are based on the PMSM system's flux linkage computations. The advantages of this method include its ease of calculation and quick dynamic reaction. The Extended Kalman Filter (EKF), MRAS, and Sliding Mode Observer (SMO) are some of the sensorless ways [7]. The drive has also been fitted with a speed controller for closed-loop sensorless control. This paper presents the closed-loop FOC of PMSM using three-level space vector pulse width modulation for reducing the harmonic distortion of output voltage, using the MRAS for observed the speed and position of PMSM and using the WOA for tuning the PI controller of closed-loop FOC this method give a good response and reduced the steady-state error.

II. THREE-LEVEL SVPWM INVERTER

To reduce harmonics in the inverter output voltage, a three-level Neutral-Point Clamped (NPC) inverter is proposed. It is impossible to connect a single switching device precisely at such high voltages. As a result, a new kind of inverter called a multilayer inverter is created. This inverter uses capacitors to divide the voltage of the direct current busses and highly powered semiconductor switches that are coupled in series. In order to produce stepped outputs, which are required for electric drive systems and are more similar to sinusoidal waveforms, the capacitor voltages are switched in a certain way. Several techniques are used in three types of classical MLI to produce these waveforms. The cascaded H bridge converters were developed to enable the acquisition of different levels from diverse DC sources. Splitting DC voltage with capacitors was another method to produce several levels from a single DC source, which led to the creation of diode-clamped MLI. The voltage across switching devices in these converters is kept below or equal to Vdc/n, where n is the number of inverter levels. To avoid the necessity for multiple rated diodes in diode-clamped MLI, the flying capacitor multilevel inverter was invented [8,9]. The NPC inverters (or Diode-Clamped inverters), Cascaded H-Bridge inverters (CHB), and Flying Capacitor (FC) inverters (or Capacitor Clamped inverters) are the three multilevel inverter topologies [10].Three Levels NPC converter contents of twelve switches and six clamped diodes. The total number of switching States is twenty-seven. They are represented by 19 fixed-position voltage vectors [11]. These switches Sa1, Sa2, and Sa3 should conduct for a Vdc/2 output voltage and a –Vdc/2 voltage, respectively. Sa4 should conduct and the switches Sa2, and Sa3 should conduct with one arm operating of phase-A for a three-level diode clamped inverter to have an output voltage of zero. Two switches should conduct at the same time at any voltage level. The output's maximum output voltage is half that of the direct current supply [12,13].

Three-level converters have the following advantages over two-level converters:

- Higher levels indicate that the output waveform is more similar to that of a sinusoidal waveform. The harmonic distortion is also reduced as a result of this.
- The voltage levels are employed at a ΔV lower level.
- The motor bearings are less strained since the clamping diodes restrict the voltage all over the OFF-state switching devices to one capacitor voltage level (half of the DC-link voltage). As a result of the reduction in voltage, medium-rated semiconductor devices can now be employed in high-voltage, high-level applications [14].

Received 01/June/2022; Accepted 18/July/2022
© 2017 University of Technology, Iraq ISSN (Print) 1811-9212 ISSN (Online) 2617-3352

DOI: https://doi.org/10.33103/uot.ijccce.23.2.4

III. MODELING OF PMSM

Fig. 1 shows the equivalent circuit of PMSM in a direct-quadratic (d-q) rotating reference frame [15].

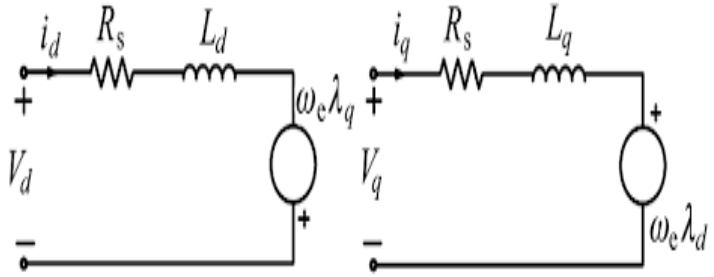

FIG. 1. EQUIVALENT CIRCUIT OF PMSM.

The stator voltages in dq reference frame is given by

$$V_d = R_s i_d + \frac{d\lambda_d}{dt} - \omega_e \lambda_q \quad (1)$$

$$V_q = R_s i_q + \frac{d\lambda_q}{dt} + \omega_e \lambda_d \quad (2)$$

Where

$$\lambda_d = L_d i_d + \lambda_f \quad (3)$$

and

$$\lambda_q = L_q i_q \quad (4)$$

The rotor-developed torque (T_e) is given by:

$$T_e = \frac{3}{2}\frac{N_p}{2}[\lambda_f i_q + (L_d - L_q) i_d i_q] \quad (5)$$

The stator currents are estimated by

$$\frac{di_d}{dt} = -\frac{R_s}{L_d} i_d + \omega_e \frac{(L_q i_q)}{L_d} + \frac{1}{L_d} V_d \quad (6)$$

$$\frac{di_q}{dt} = -\frac{R_s}{L_q} i_q - \omega_e \frac{(L_d i_d + \lambda_f)}{L_q} + \frac{1}{L_q} V_q \quad (7)$$

The rotor speed is estimated for the resultant torque or

$$\frac{d\omega_r}{dt} = \frac{T_e - T_m - F\omega_r}{J} \quad (8)$$

$$\omega_e = \frac{N_p}{2} \quad (9)$$

IV. SENSORLESS CONTROL OF PMSM

Sensorless control is a variation of the FOC algorithm that allows synchronous motors to run without using mechanical speed sensors. Because these sensors are infamous for breaking, removing them lowers the motor's cost and size while also improving the drive's long-term accuracy and dependability. This is especially crucial if the motor is going to be operated in a harsh, inaccessible area, like an oil well. Control engineers can calculate values from a system's state variables instead of directly measuring them. The state space modeling methodology is a useful tool for studying and regulating complicated nonlinear systems with various inputs and outputs [16]. MRAS is one of the sensorless control estimation approaches.

Received 01/June/2022; Accepted 18/July/2022
© 2017 University of Technology, Iraq
ISSN (Print) 1811-9212 ISSN (Online) 2617-3352

DOI: https://doi.org/10.33103/uot.ijccce.23.2.4

V. SENSORLESS MRAS

The MRAS algorithm is basic and adapts quickly. In a digital control system, this is simple to accomplish. The MRAS is made up of three parts: a reference model, an adaptive model, and an adaptive rule. The reference model represents the PMSM model. The adaptive model is the current equations model with estimated variables. The results of both models have the same physical relevance. The unknown parameters can be found by using the adaptive rule to process the error of the two outputs [17].

Equation (10) shows the voltages and currents in matrix form as:

$$\frac{d}{dt}\begin{bmatrix} i_d \\ i_q \end{bmatrix} = \begin{bmatrix} \frac{-R_s}{L_s} & \omega_r \\ -\omega_r & \frac{-R_s}{L_s} \end{bmatrix}\begin{bmatrix} i_d \\ i_q \end{bmatrix} + \frac{1}{L_s}\begin{bmatrix} u_d \\ u_q \end{bmatrix} \quad (10)$$

$$\text{Where A}=\begin{bmatrix} \frac{-R_s}{L_s} & \omega_r \\ -\omega_r & \frac{-R_s}{L_s} \end{bmatrix} \quad (11)$$

Let

$$i'_d = i_d + \frac{\lambda_f}{Ls}\ ;\ i'_q = i_q \quad (12)$$

$$u'_d = u_d + \frac{R\lambda_f}{Ls}\ ;\ u'_q = u_q \quad (13)$$

The speed estimator can be described by

$$\frac{d}{dt}\begin{bmatrix} \hat{i}'_d \\ \hat{i}'_q \end{bmatrix} = \begin{bmatrix} \frac{-R_s}{L_s} & \widehat{\omega}_r \\ \widehat{\omega}_r & \frac{-R_s}{L_s} \end{bmatrix}\begin{bmatrix} \hat{i}'_d \\ \hat{i}'_q \end{bmatrix} + \frac{1}{Ls}\begin{bmatrix} u'_d \\ u'_q \end{bmatrix} \quad (14)$$

Let $e=i' - \hat{i}'$ is the error of the static variable. The following equations can be written as follows:

$$\frac{d}{dt}\hat{i}' = \hat{A}\hat{i}' + Bu' \quad (15)$$

The estimated rotor speed is given by

$$\widehat{\omega}_r = \int k_1 (i'_d\hat{i}'_q - i'_q\hat{i}'_d)\, dt + k_2(i'_d\hat{i}'_q - i'_q\hat{i}'_d) + \widehat{\omega}_r(0) \quad (16)$$

$$\widehat{\omega}_r = \int k_1 [i'_d\hat{i}_q - i'_q\hat{i}_d - \frac{\lambda_f}{L}(i_q - \hat{i}_q)]\, dt + k_2[i_d\hat{i}_q - i_q\hat{i}_d\frac{\lambda_f}{Ls}(i_q - \hat{i}_q)] + \widehat{\omega}_r(0) \quad (17)$$

VI. WHALE OPTIMIZATION ALGORITHM

Mirjalili and Lewis developed the WOA in 2016, which is a mimic of the humpback whale's social behavior [18]. The Whale Optimization Algorithm is triggered by humpback whales' hunting behavior and their use of a bubble-net approach for hunting [19]. The bubble-net searching approach developed the method. Humpback whales' hunting habits inspired this piece. The bubble-net feeding method is a foraging strategy used by humpback whales, in which they form characteristic bubbles in a curved shape around the prey from about 12 meters below the surface, encircling animals, and then swimming up to the surface to begin chasing them [20-21]. Humpback whales are capable of identifying the prey's location and surrounding them. Since the best design position in the search space is unidentified in advance, the best instantaneous response, according to the Whale Optimization Algorithm, is the designated prey or something close to it. Once the finest searcher has been identified, the other searchers will attempt to update their locations in the direction of the finest searcher. This behavior is denoted by the next equalities:

$$\vec{D} = \left|\vec{C}.\vec{X}_p(t) - \vec{X}(t)\right| \quad (18)$$

$$\vec{X}_p(t+1) = \vec{X}_p(t) - \vec{A}.\vec{D} \quad (19)$$

Received 01/June/2022; Accepted 18/July/2022
© 2017 University of Technology, Iraq ISSN (Print) 1811-9212 ISSN (Online) 2617-3352

DOI: https://doi.org/10.33103/uot.ijccce.23.2.4

Where t is the current iteration of the search, $\vec{X}_p$ denotes the prey position vector, $\vec{X}$ denotes the whale location vector, and $\vec{A}$ and $\vec{C}$ denote coefficient vectors derived as:

$$\vec{A} = 2\vec{a}.\vec{r}_1 - \vec{a} \quad (20)$$

$$\vec{C} = 2.\vec{r}_2 \quad (21)$$

Where $\vec{r}_1$ and $\vec{r}_2$ are arbitrary vectors in [0, 1], and the components of $\vec{a}$ are reduced linearly from 2 to 0 across the sequence of repeats. Humpback whales swim by closing a circle and swimming in a helical pattern at the same time to circulate their target. A 50% chance of determining whether the spiral process is locked or the location of the whales is considered to represent this behavior concurrently. The modeling algebraic that simulates the preceding procedure is as follows:

$$x(t+1) = \begin{cases} x^*(t) - A.D & if\ p \geq 0.5 \\ D.e^{bI}.cos(2L\pi) + x^*(t) & if\ x \geq 0.5 \end{cases} \quad (22)$$

Where b is steady which describes the logarithmic helical form, l is an arbitrary value in the range of [-1, 1], and p is an arbitrary number in the range of [0, 1]. Search agents change their locations for an arbitrarily selected search agent or the finest solution obtained in each cycle. To provide exploration and exploitation, the value is lowered from 2 to 0 [22]. *Fig. 2* shows the flowchart of WOA.

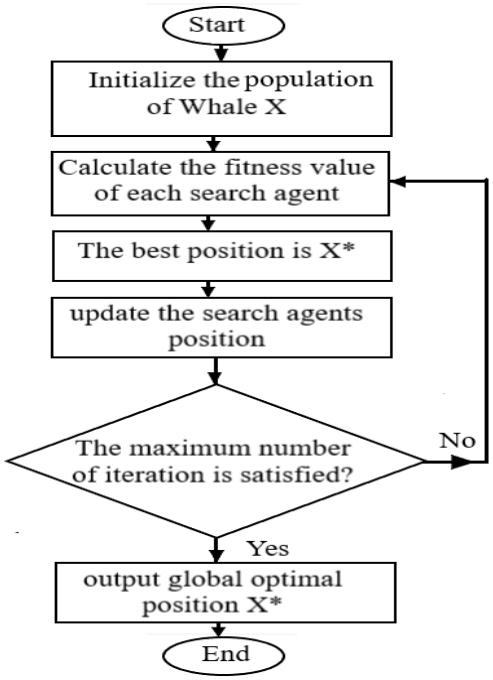

FIG. 2. FLOWCHART OF WOA.

VII. RESULTS AND DISCUSSION

The Simulink model of PMSM is shown in *Fig. 3*. The Parameters of the PMSM model are: stator resistance Rs=2.6 Ω, q and d inductances are Lq=Ld=Ls=0.043H, combined inertia of the rotor and load J =0.000085 kg·m2; combined viscous friction of rotor and load F=0.001, induced flux by the permanent magnets of the rotor in the stator phases $\boldsymbol{\lambda_f}$ =0.175Wb; and pole pairs number P=2.

Received 01/June/2022; Accepted 18/July/2022
© 2017 University of Technology, Iraq
ISSN (Print) 1811-9212 ISSN (Online) 2617-3352

DOI: https://doi.org/10.33103/uot.ijccce.23.2.4

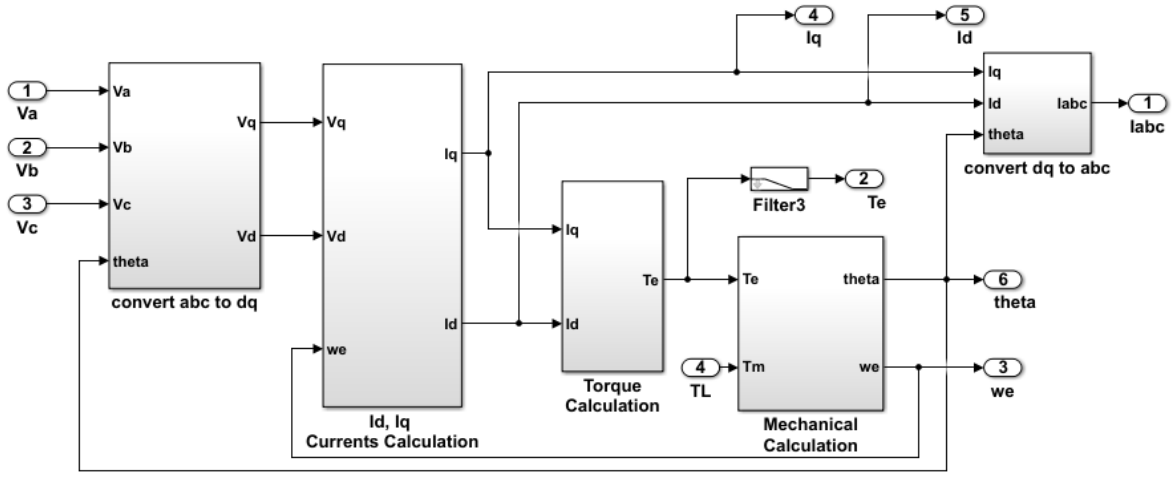

FIG. 3. SIMULINK MODEL OF THE PERMANENT MAGNET SYNCHRONOUS MOTOR (PMSM).

Fig. 4 shows the Simulink model of a three-level SVPWM inverter. Vector selection in the q-d stationary reference frame is the basis for SVM. The three closest vectors are identified first in the SVM scheme. Clark's Transformation can be used to determine the magnitude and angle of the spinning vector. The voltage is used to implement the space vector PWM. Equations in the a-b-c reference frame can be converted to the stationary d-q reference frame, which is made up of the vertical (q) and horizontal (d) axes PWM signals are generated using the SVPWM system, which is based on sampling amplitudes of voltages of reference phase Waveforms of line voltage, line current, and THD for line voltage and line current Three level inverter simulation circuit model for SVPWM generator inverter operation is shown. *Fig. 4* shows the circuit of the three-level inverter. The typical architecture of a diode-clamped (neutral-point clamped) three-level inverter is shown in *Fig. 5*. The system has 12 power switching devices (such as Sl-S4) and 6 diodes clamped. There are 27 in total, as indicated in diode-clamped three-level inverter switching states. They correspond to 19 voltage vectors.

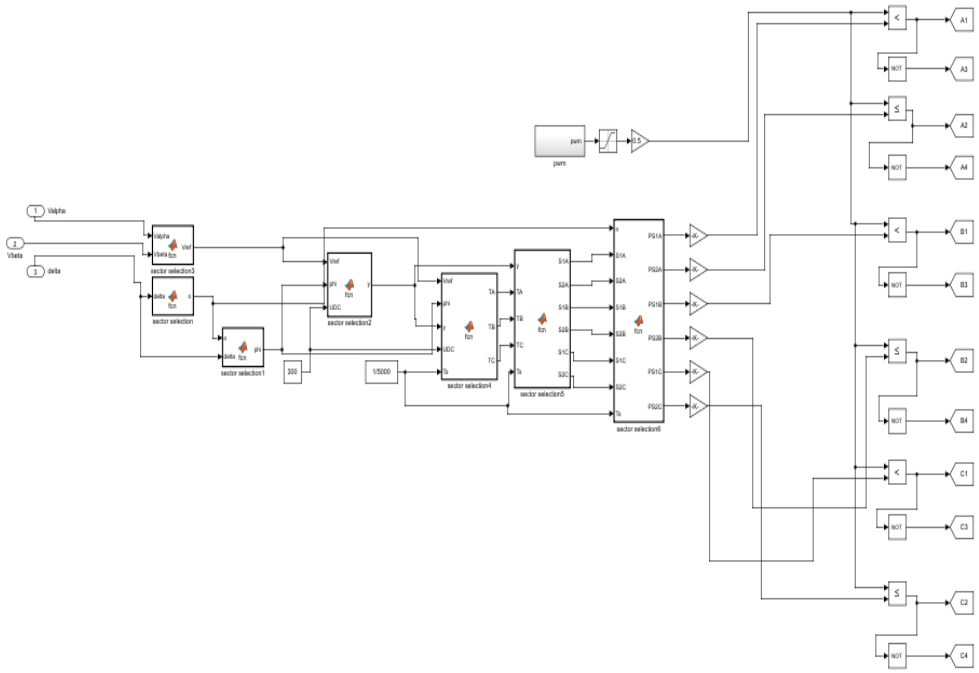

FIG. 4. SIMULATION CIRCUIT OF 3-LEVEL INVERTER FOR SVPWM.

Received 01/June/2022; Accepted 18/July/2022
© 2017 University of Technology, Iraq
ISSN (Print) 1811-9212 *ISSN (Online) 2617-3352*

DOI: https://doi.org/10.33103/uot.ijccce.23.2.4

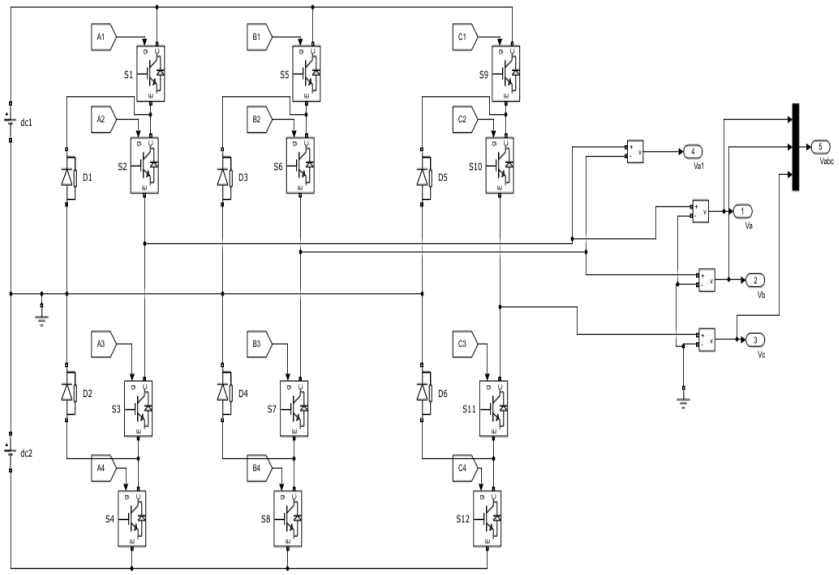

FIG. 5. THREE-LEVEL DIODE CLAMPED INVERTER.

Fig. 6 illustrates the Simulink MRAS configurable. It calculates the currents in the d-q frame by combining the applied stator voltages with a speed estimate. The adjustment process to the right in the figure then uses the estimated values. To fine-tune the speed estimate using currents and observed currents the predicted speed the "speed estimate" signal is fed back into the customized model, which produces an approximated speed value. The speed estimation signal is also used to obtain a position.

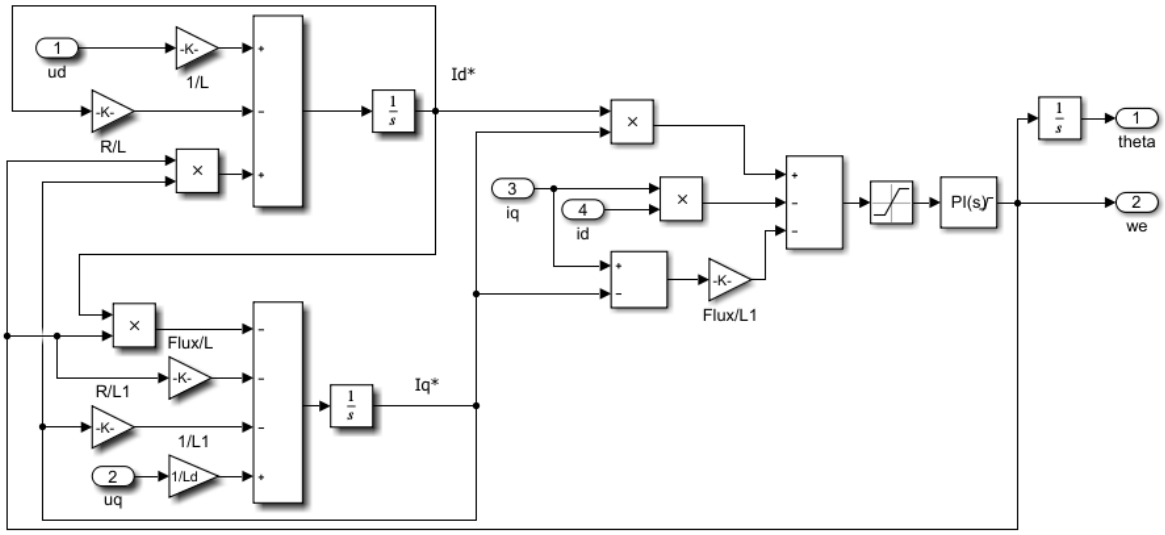

FIG. 6. COMPLETE SIMULINK MODEL OF MRAS OBSERVER.

Fig. 7 shows the Simulink model of sensorless FOC, this model of FOC uses the park and Clark transformation uses the three-level SVPWM inverter and uses the estimated method MRAS.

Received 01/June/2022; Accepted 18/July/2022
© 2017 University of Technology, Iraq
ISSN (Print) 1811-9212 *ISSN (Online) 2617-3352*

DOI: https://doi.org/10.33103/uot.ijccce.23.2.4

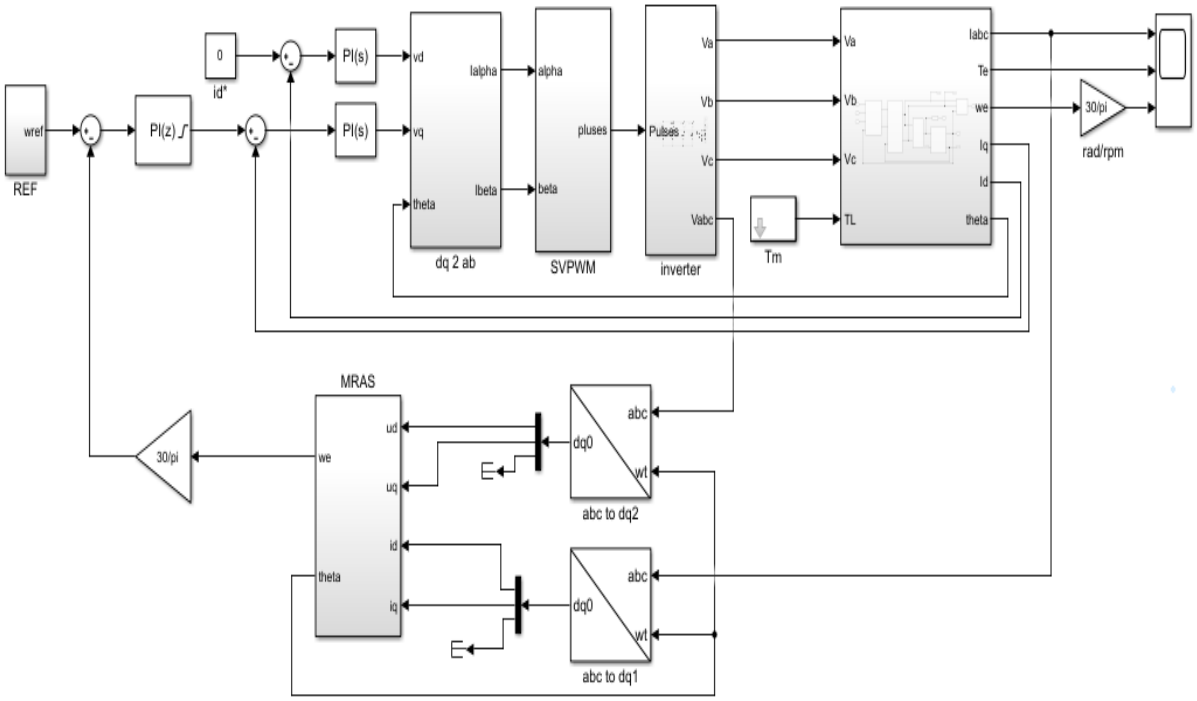

FIG. 7. SIMULINK MODEL OF PMSM SENSORLESS FIELD-ORIENTED CONTROL SYSTEM.

Fig. 8 shows the output voltage of the three-level SVPWM inverter when using the dc voltages is 300 volts. *Fig. 9* shows the three-phase Currents response using classical FOC of three-level SVPWM. The motor is at half loading at starting instant and the stator current value with 2 amperes. Loading instant at t=2 sec, the stator current values become 6 amperes. *Fig. 10* depicts the torque created in the rotor the load torque at the start is 1 N m and when the full load at 2 seconds becomes 2 N m when shown in this figure.

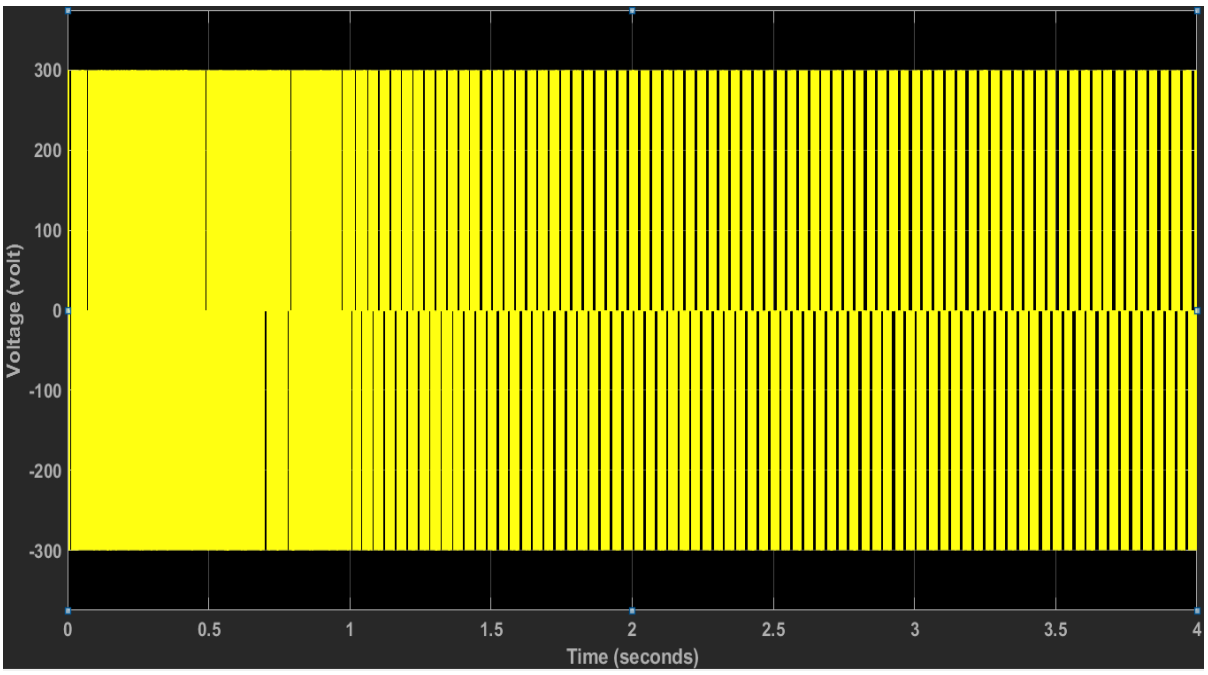

FIG. 8. OUTPUT VOLTAGE WAVEFORMS OF 3-LEVEL SVPWM MULTI-INVERTER.

Received 01/June/2022; Accepted 18/July/2022
© 2017 University of Technology, Iraq
ISSN (Print) 1811-9212 *ISSN (Online) 2617-3352*

DOI: https://doi.org/10.33103/uot.ijccce.23.2.4

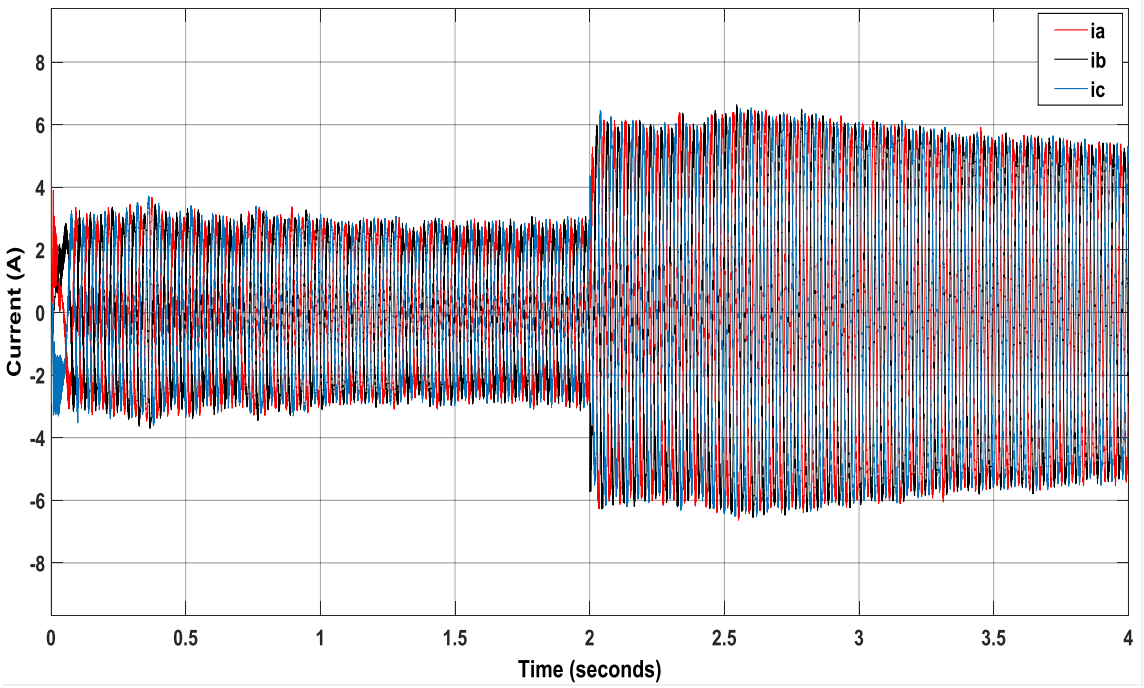

FIG. 9. THREE-PHASE CURRENTS RESPONSE.

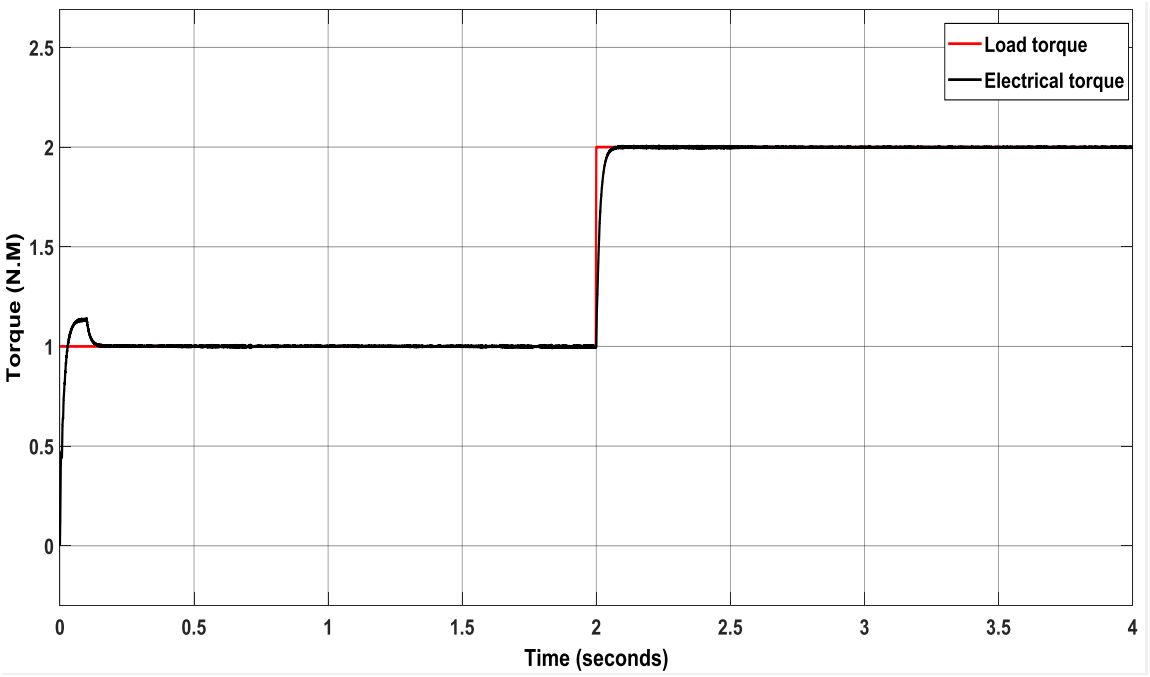

FIG. 10. TORQUE RESPONSE OF THE DRIVE.

Fig. 11 demonstrates the sensorless vector control simulation platform of PMSM based on this approach employing traditional FOC of three-level SVPWM, MATLAB, and this algorithm. The utilization of permanent magnet synchronous motor characteristics is one of them. The rated speed is 1500 rpm. The anticipated speed of the motor and the actual speed curve during the motor starting phase when comparing the three curves, it is clear that the MRAS algorithm can accurately predict motor

Received 01/June/2022; Accepted 18/July/2022
© 2017 University of Technology, Iraq
ISSN (Print) 1811-9212 ISSN (Online) 2617-3352

DOI: https://doi.org/10.33103/uot.ijccce.23.2.4

speed during the motor beginning phase. The projected speed closely matches the motor's real speed. When the load torque is applied at a time of 2 seconds, the anticipated speed becomes a simple oscillation and then smooth responses.

The WOA is performed with the parameters that are shown in Table I. The fitness function of WOA is shown in *Fig. 12*. The enhancement of system response due to the three-level inverter is listed in Table II. *Fig. 13* depicts the performance of a PMSM drive while utilizing a whale optimization algorithm (WOA) adjusted PI controller to apply braking to the motor. When the reference speed is reversed to 1500 rpm in *Fig. 11*, the rotor speed follows suit and reaches the same speed of 1500 rpm. The speed response is smoother when using the clever PI controller than when using the try-and-error method (classical method). When comparing the actual and estimated rotor angles, *Fig. 14* illustrates the rotor angle. *Fig. 15* shows the Estimated Speed response using classical FOC and optimal FOC based on three-level SVPWM.

TABLE I. PARAMETERS OF WOA

r1	Random values between [0 1]
r2	Random values between [0 1]
Dimension	8
Number of iterations	100
Srearch agents	5

TABLE II. SPEED RESPONSES OF CLASSICAL FOC BASED ON THREE-LEVEL SVPWM.

Speed Response	Value
Overshoot	1.318%
Undershoot	1.998%
Rise time	30.883 ms
Steady-state error	0.2N.m

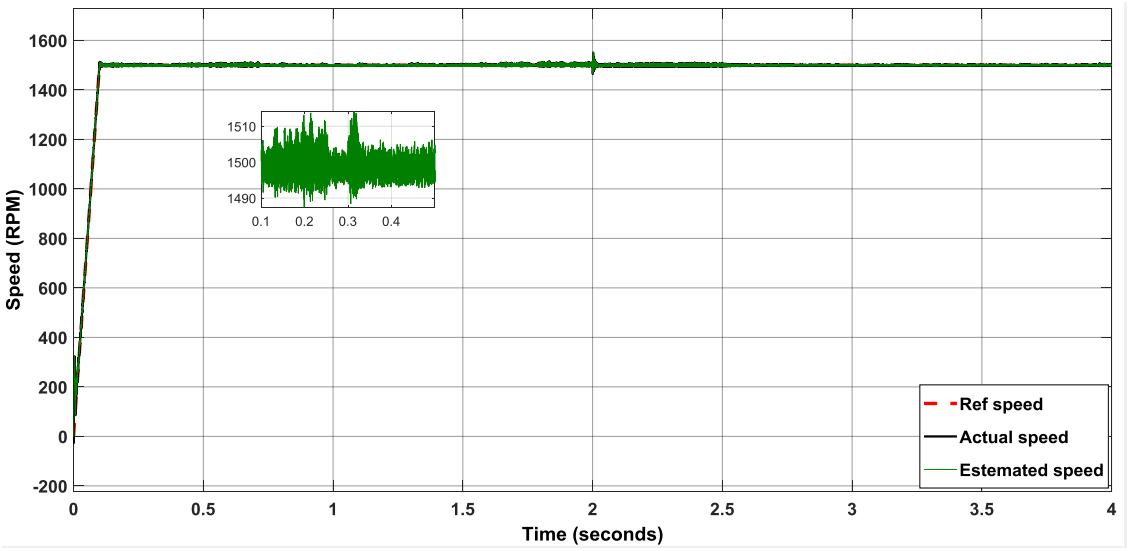

FIG. 11. SPEED RESPONSE USING CLASSICAL FOC.

Received 01/June/2022; Accepted 18/July/2022
© 2017 University of Technology, Iraq
ISSN (Print) 1811-9212 *ISSN (Online) 2617-3352*

DOI: https://doi.org/10.33103/uot.ijccce.23.2.4

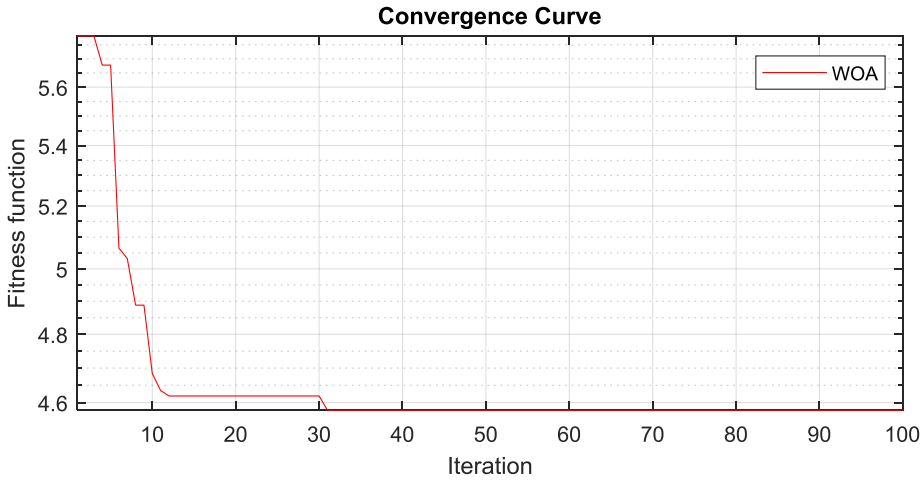

FIG. 12. ITAE PERFORMANCE INDEX OF THE OPTIMIZATION PROCESS.

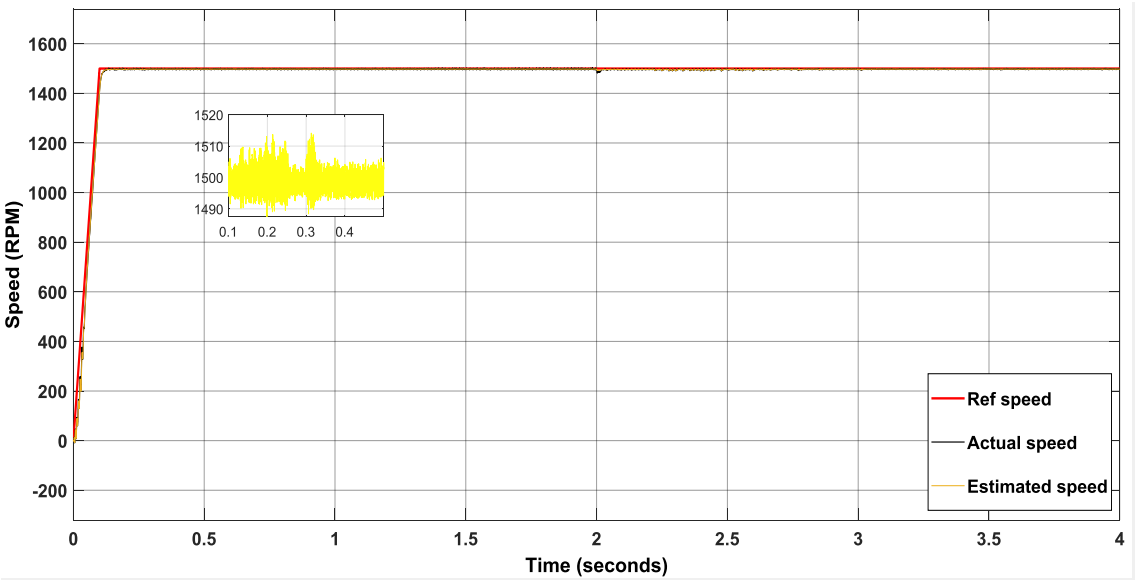

FIG. 13. SPEED RESPONSE USING OPTIMAL FOC.

TABLE III. SPEED RESPONSES OF OPTIMAL FOC BASED ON THREE-LEVEL SVPWM

Speed Response	Value
Overshoot	0.943%
Undershoot	2.00%
Rise time	12.561 ms
Steady-state error	0.05N.m

Received 01/June/2022; Accepted 18/July/2022
© 2017 University of Technology, Iraq
ISSN (Print) 1811-9212 *ISSN (Online) 2617-3352*

DOI: https://doi.org/10.33103/uot.ijccce.23.2.4

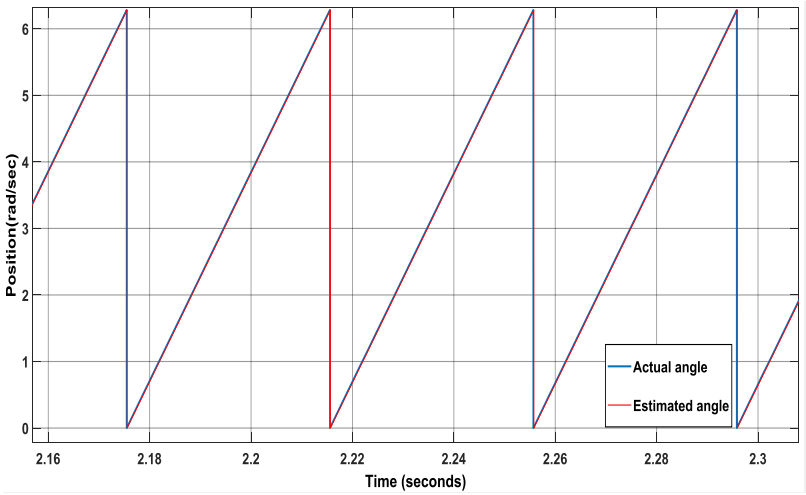

FIG. 14. ROTOR POSITION.

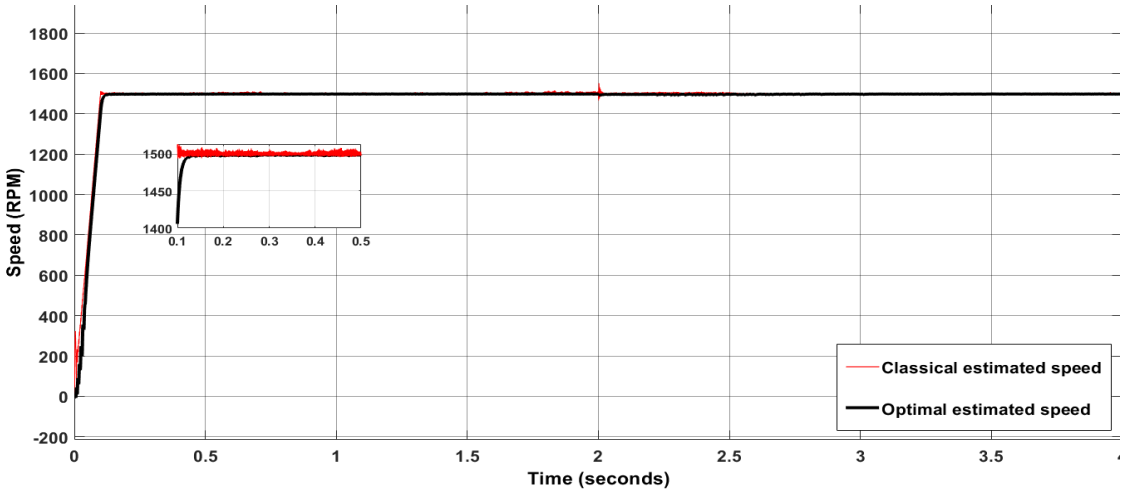

FIG. 15. ESTIMATED SPEED RESPONSE USING CLASSICAL FOC AND OPTIMAL FOC.

VIII. CONCLUSIONS

In this paper, sensorless speed control based on MRAS with a three-level SVPWM algorithm is proposed. Simulation results show that the inverter harmonic components are reduced. The MRAS estimates the rotor speed and rotor position accurately. The WOA is a powerful meta-heuristic optimization method that is used to enhance the estimator process. The obtained results show an improvement in motor performance when using PI-WOA compared to classical PI controllers. This method can improve the performance of the system compared with the classical trial and error method in terms of reducing steady-state error, overshoot, rise time, and smoother response to make this controller more robust to variation in load other than the rest motor controllers. The FOC response is modified according to a good estimation performed by intelligent MRAS and the minimization of THD of the inverter. Minimum harmonics lead to no need for using the filter at the inverter output.

Received 01/June/2022; Accepted 18/July/2022
© 2017 University of Technology, Iraq
ISSN (Print) 1811-9212 *ISSN (Online) 2617-3352*

DOI: https://doi.org/10.33103/uot.ijccce.23.2.4

APPENDIX

NOMENCLATURE

Symbol	Definition	Units
F	Friction coefficient	**None**
i_d, i_q	Currents in d-q axis	Amperes
J	Inertial moment	Kg $* m^2$
L_d, L_q	d- q axis inductances	Henry
N_p	Number of pole pairs	None
R_s	Stator resistance	Ohms
T_e	Electromagnetic torque	N m
V_d, V_q	Voltage in d- q axis voltages	Volts
λ_q, λ_q	The d-q axis flux-linkages	Weber
λ_f	Induced flux	Weber
w_r	The mechanical angular speed	radians per second
w_e	The stator electrical angular speed	radians per second
L_s	Stator winding self-inductance	Henry

REFERENCES

[1] M. Rasheed, R. Omar, M. Sulaiman, A. Aljanad, and A. Ahmad, "Performance studies of three-phase cascaded H-Bridge and Diode-Clamped multilevel inverters," in *CEAT 2013 - 2013 IEEE Conference on Clean Energy and Technology*, 2013, pp. 281–286, doi: 10.1109/CEAT.2013.6775641.

[2] I. Ahmed and V. B. Borghate, "Simplified space vector modulation technique for seven-level cascaded H-bridge inverter," *IET Power Electron.*, vol. 7, no. 3, pp. 604–613, 2014, doi: 10.1049/iet-pel.2013.0135.

[3] H. Yao, Y. Yan, T. Shi, G. Zhang, Z. Wang, and C. Xia, "A Novel SVPWM Scheme for Field-Oriented Vector-Controlled PMSM Drive System Fed by Cascaded H-Bridge Inverter," *IEEE Trans. Power Electron.*, vol. 36, no. 8, pp. 8988–9000, 2021, doi: 10.1109/TPEL.2021.3054642.

[4] T. A. Ahmed, E. Mohamed, A. Youssef, and A. A.Ibrahim, "Review of Permanent Magnet Synchronous Motor Fed by Multilevel Inverter," *SVU-International J. Eng. Sci. Appl.*, vol. 1, no. 1, pp. 22–31, 2020, doi: 10.21608/svusrc.2020.51244.1001.

[5] L. A. Mohammed, "Permanent Magnet Synchronous Motor Drive Based on Maximum boost control Z-source SVPWM," *Zanco J. Pure Appl. Sci.*, vol. 31, no. s3, 2019, doi: 10.21271/zjpas.31.s3.24.

[6] M. Nicola and C. I. Nicola, "Sensorless Predictive Control for PMSM Using MRAS Observer," *2019 Int. Conf. Electromechanical Energy Syst. SIELMEN 2019 - Proc.*, vol. 2, no. 1, pp. 59–67, 2019, doi: 10.1109/SIELMEN.2019.8905815.

[7] H. Lin *et al.*, "MRAS-Based Sensorless Control of PMSM with BPN in Prediction Mode," *IEEE Int. Symp. Ind. Electron.*, vol. 2019-June, no. June, pp. 1755–1760, 2019, doi: 10.1109/ISIE.2019.8781197.

[8] I. Ahmed and V. B. Borghate, "Simplified space vector modulation technique for seven-level cascaded H-bridge inverter," *IET Power Electron.*, vol. 7, no. july, pp. 604–613, 2014, doi: 10.1049/iet-pel.2013.0135.

[9] N. Susheela, P. S. Kumar, and S. K. Sharma, "Generalized Algorithm of Reverse Mapping based SVPWM Strategy for Diode Clamped Multilevel Inverters," *IEEE Trans. Ind. Appl.*, vol. 54, pp. 2425–2437, 2018, doi: 10.1109/TIA.2018.2790906.

[10] M. Rasheed, R. Omar, M. Sulaiman, and A. Aljanad, "Performance Studies of Three-Phase Cascaded H- Bridge and Diode-Clamped Multilevel inverters," no. August 2015, 2013, doi: 10.1109/CEAT.2013.6775641.

[11] M. Soleimanipour, H. S. Goughari, and N. Sargolzaei, "Analysis and comparison of multi-level inverters based on two-level space vector PWM," *Proc. - 2012 14th Int. Conf. Model. Simulation, UKSim 2012*, vol. 0, pp. 464–469, 2012, doi: 10.1109/UKSim.2012.70.

[12] M. Murnane and I. S. Ono, "Simulink-Based SVPWM Current Control Technique for Multilevel Diode NPC Inverter Topologies."

[13] R. G. Shriwastava, M. B. Daigavane, and P. M. Daigavane, "Simulation Analysis of Three Level Diode Clamped Multilevel Inverter Fed PMSM Drive Using Carrier Based Space Vector Pulse Width Modulation (CB-SVPWM)," in

Received 01/June/2022; Accepted 18/July/2022
© 2017 University of Technology, Iraq *ISSN (Print) 1811-9212* *ISSN (Online) 2617-3352*

DOI: https://doi.org/10.33103/uot.ijccce.23.2.4

Procedia Computer Science, 2016, vol. 79, no. Dcml, pp. 616–623, doi: 10.1016/j.procs.2016.03.078.

[14] J. Dario Betanzos Ramirez, J. Jose Rodríguez Rivas, and E. Peralta Sanchez, "Space vector pulse width modulation for three-level NPC-VSI," *IEEE Lat. Am. Trans.*, vol. 11, no. 2, pp. 759–767, 2013, doi: 10.1109/TLA.2013.6533965.

[15] H. W. K. Farazdaq R. Yasien, "Sensorless speed estimation of permanent magnet synchronous motor," *Proc. - 2018 Int. Conf. Mechatronics Control. ICMC 2018*, vol. 18, no. 1, pp. 1142–1147, 2018, doi: 10.1109/ICMC.2014.7231731.

[16] G. Taha and A. Abd, "Study and Comparison The Performance of Sensorless Control of PMSM Drive System," *Eng. Technol. J.*, vol. 32, no. 10, 2014.

[17] J. Xu, B. Xu, W. Ji, G. Shi, and S. Ding, "Research on speed sensorless operation of PMSM based on improved MRAS," *2017 Asian Control Conf. ASCC 2017*, vol. 2018-Janua, pp. 1423–1427, 2018, doi: 10.1109/ASCC.2017.8287381.

[18] D. Mokeddem and S. Mirjalili, "Improved Whale Optimization Algorithm applied to design PID plus second-order derivative controller for automatic voltage regulator system," *J. Chinese Inst. Eng. Trans. Chinese Inst. Eng.* vol. 00, no. 00, pp. 1–12, 2020, DOI: 10.1080/02533839.2020.1771205.

[19] A. A. Al-Qassar *et al.*, "Finite-time control of wing-rock motion for delta-wing aircraft based on a whale-optimization algorithm," *Indones. J. Sci. Technol.*, vol. 6, no. 3, pp. 441–456, 2021, DOI: 10.17509/ijost.v6i3.37922.

[20] K. S. Simhadri, B. Mohanty, and S. K. Panda, "Comparative performance analysis of 2DOF state feedback controller for automatic generation control using a whale optimization algorithm," *Optim. Control Appl. Methods*, vol. 40, no. 1, pp. 24–42, 2019, DOI: 10.1002/oca.2462.

[21] O. Aguilar-Mejía, H. Minor-Popocatl, and R. Tapia-Olvera, "Comparison and ranking of metaheuristic techniques for optimization of PI controllers in a machine drive system," *Appl. Sci.*, vol. 10, no. 18, 2020, DOI: 10.3390/APP10186592.

[22] C. J. Parvathy, A. Haseena, and P. Abraham, "Grey wolf optimizer based speed control of permanent magnet synchronous motor," *AIP Conf. Proc.*, vol. 2222, no. April 2020, DOI: 10.1063/5.0003947.

Received 01/June/2022; Accepted 18/July/2022
© 2017 University of Technology, Iraq *ISSN (Print) 1811-9212* *ISSN (Online) 2617-3352*